



HAL
open science

Influence of polarimetric satellite data measured in the visible region on aerosol detection and on the performance of atmospheric correction procedure over open ocean waters

Tristan Harmel, Malik Chami

► To cite this version:

Tristan Harmel, Malik Chami. Influence of polarimetric satellite data measured in the visible region on aerosol detection and on the performance of atmospheric correction procedure over open ocean waters. *Optics Express*, 2011, 19 (21), pp.20960-20983. 10.1364/OE.19.020960 . hal-03502013

HAL Id: hal-03502013

<https://hal.science/hal-03502013>

Submitted on 29 Dec 2023

HAL is a multi-disciplinary open access archive for the deposit and dissemination of scientific research documents, whether they are published or not. The documents may come from teaching and research institutions in France or abroad, or from public or private research centers.

L'archive ouverte pluridisciplinaire **HAL**, est destinée au dépôt et à la diffusion de documents scientifiques de niveau recherche, publiés ou non, émanant des établissements d'enseignement et de recherche français ou étrangers, des laboratoires publics ou privés.



Distributed under a Creative Commons Attribution 4.0 International License

Influence of polarimetric satellite data measured in the visible region on aerosol detection and on the performance of atmospheric correction procedure over open ocean waters

Tristan Harmel^{1,2,*} and Malik Chami^{1,2,3}

¹Université Pierre et Marie Curie, Laboratoire Océanographie de Villefranche, 06230 Villefranche sur Mer, France

²CNRS, Laboratoire Océanographie de Villefranche Villefranche sur Mer, France

³Institut Universitaire de France

*tharmel@ccny.cuny.edu

Abstract: An original atmospheric correction algorithm, so-called *multi-directionality and POLarization-based Atmospheric Correction* (POLAC), is described. This algorithm is based on the characteristics of the multidirectional and polarimetric data of the satellite PARASOL (CNES). POLAC algorithm is used to assess the influence of the polarimetric information in the visible bands on the retrieval of the aerosol properties and the water-leaving radiance over open ocean waters. This study points out that the use of the polarized signal significantly improves the aerosol type determination. The use of the polarized information at one visible wavelength only, namely 490 nm, allows providing estimates of the Angstrom exponent of aerosol optical depth with an uncertainty lower than 4%. Based on PARASOL observations, it is shown that the detection of the fine aerosols is improved when exploiting polarization data. The atmospheric component of the satellite signal is then better modeled, thus improving *de facto* the water-leaving radiance estimation.

©2011 Optical Society of America

OCIS codes: (010.1285) Atmospheric correction; (010.1110) Aerosols; (260.5430) Polarization; (120.0280) Remote sensing and sensors; (010.0010) Atmospheric and oceanic optics.

References and links

1. S. Alvain, C. Moulin, Y. Dandonneau, and F. M. Bréon, "Remote sensing of phytoplankton groups in case 1 waters from global SeaWiFS imagery," *Deep Sea Res. Part I Oceanogr. Res. Pap.* **52**(11), 1989–2004 (2005).
2. M. Doron, M. Babin, A. Mangin, and O. Hembise, "Estimation of light penetration, and horizontal and vertical visibility in oceanic and coastal waters from surface reflectance," *J. Geophys. Res.- Oceans* **112**(C6), C06003 (2007).
3. IOCCG, *Why Ocean Colour? The Societal Benefits of Ocean-Colour Technology*, T. Platt, N. Hoepffner, V. Stuart, and C. Brown, eds, Reports of the International Ocean-Colour Coordinating Group, 7 (IOCCG, 2008).
4. M. J. Behrenfeld, R. T. O'Malley, D. A. Siegel, C. R. McClain, J. L. Sarmiento, G. C. Feldman, A. J. Milligan, P. G. Falkowski, R. M. Letelier, and E. S. Boss, "Climate-driven trends in contemporary ocean productivity," *Nature* **444**(7120), 752–755 (2006).
5. J. J. Polovina, E. A. Howell, and M. Abecassis, "Ocean's least productive waters are expanding," *Geophys. Res. Lett.* **35**(3), L03618 (2008).
6. E. Martinez, D. Antoine, F. D'Ortenzio, and B. Gentili, "Climate-driven basin-scale decadal oscillations of oceanic phytoplankton," *Science* **326**(5957), 1253–1256 (2009).
7. IOCCG, *Atmospheric Correction for Remotely-Sensed Ocean-Colour Products* M. Wang, D. Antoine, P. Y. Deschamps, R. Frouin, H. Fukushima, H. R. Gordon, A. Morel, J. M. Nicolas, and V. Stuart, eds, Reports of the International Ocean-Colour Coordinating Group, No. 10 (IOCCG, 2010).
8. M. D. King, Y. J. Kaufman, D. Tanre, and T. Nakajima, "Remote sensing of tropospheric aerosols from space: past, present, and future," *Bull. Am. Meteorol. Soc.* **80**, 2229–2259 (1999).

9. Z. Ahmad, B. A. Franz, C. R. McClain, E. J. Kwiatkowska, J. Werdell, E. P. Shettle, and B. N. Holben, "New aerosol models for the retrieval of aerosol optical thickness and normalized water-leaving radiances from the SeaWiFS and MODIS sensors over coastal regions and open oceans," *Appl. Opt.* **49**(29), 5545–5560 (2010).
10. D. Antoine and A. Morel, "A multiple scattering algorithm for atmospheric correction of remotely sensed ocean colour (MERIS instrument): principle and implementation for atmospheres carrying various aerosols including absorbing ones," *Int. J. Remote Sens.* **20**(9), 1875–1916 (1999).
11. H. R. Gordon, "Atmospheric correction of ocean color imagery in the Earth Observing System era," *J. Geophys. Res.* **102**(D14), 17081–17106 (1997).
12. H. Fukushima, A. Higurashi, Y. Mitomi, T. Nakajima, T. Noguchi, T. Tanaka, and M. Toratani, "Correction of atmospheric effects on ADEOS/OCTS ocean color data: algorithm description and evaluation of its performance," *J. Oceanogr.* **54**(5), 417–430 (1998).
13. H. R. Gordon and M. Wang, "Retrieval of water-leaving radiance and aerosol optical thickness over the oceans with seaWiFS: a preliminary algorithm," *Appl. Opt.* **33**(3), 443–452 (1994).
14. F. Mélin, M. Clerici, G. Zibordi, B. N. Holben, and A. Smirnov, "Validation of SeaWiFS and MODIS aerosol products with globally distributed AERONET data," *Remote Sens. Environ.* **114**(2), 230–250 (2010).
15. F. Mélin and G. Zibordi, "Vicarious calibration of satellite ocean color sensors at two coastal sites," *Appl. Opt.* **49**(5), 798–810 (2010).
16. D. Antoine, F. d'Ortenzio, S. B. Hooker, G. Bécu, B. Gentili, D. Tailliez, and A. J. Scott, "Assessment of uncertainty in the ocean reflectance determined by three satellite ocean color sensors (MERIS, SeaWiFS and MODIS-A) at an offshore site in the Mediterranean Sea (BOUSSOLE project)," *J. Geophys. Res.* **113**(C7), C07013 (2008).
17. M. Chami, "Importance of the polarization in the retrieval of oceanic constituents from the remote sensing reflectance," *J. Geophys. Res. - Oceans* **112**(C5), C05026 (2007).
18. T. Harmel and M. Chami, "Invariance of polarized reflectance measured at the top of atmosphere by PARASOL satellite instrument in the visible range with marine constituents in open ocean waters," *Opt. Express* **16**(9), 6064–6080 (2008).
19. J. Chowdhary, B. Cairns, and L. D. Travis, "Case studies of aerosol Retrievals over the ocean from multiangle, multispectral photopolarimetric remote sensing data," *J. Atmos. Sci.* **59**(3), 383–397 (2002).
20. M. I. Mishchenko and L. D. Travis, "Satellite retrieval of aerosol properties over the ocean using measurements of reflected sunlight: Effect of instrumental errors and aerosol absorption," *J. Geophys. Res. - Atmos.* **102**(D12), 13543–13553 (1997).
21. M. I. Mishchenko and L. D. Travis, "Satellite retrieval of aerosol properties over the ocean using polarization as well as intensity of reflected sunlight," *J. Geophys. Res. - Atmos.* **102**(D14), 16989–17013 (1997).
22. V. Zubko, Y. J. Kaufman, R. I. Burg, and J. V. Martins, "Principal component analysis of remote sensing of aerosols over oceans," *IEEE Trans. Geosci. Remote Sensing* **45**(3), 730–745 (2007).
23. M. I. Mishchenko, I. V. Geogdzhayev, B. Cairns, B. E. Carlson, J. Chowdhary, A. A. Lacis, L. Liu, W. B. Rossow, and L. D. Travis, "Past, present, and future of global aerosol climatologies derived from satellite observations: A perspective," *J. Quant. Spectrosc. Radiat. Transf.* **106**(1-3), 325–347 (2007).
24. P. Y. Deschamps, F. M. Breon, M. Leroy, A. Podaire, A. Bricaud, J. C. Buriez, and G. Seze, "The polder mission - instrument characteristics and scientific objectives," *IEEE Trans. Geosci. Remote Sensing* **32**(3), 598–615 (1994).
25. J. L. Deuzé, F. M. Breon, C. Devaux, P. Goloub, M. Herman, B. Lafrance, F. Maignan, A. Marchand, F. Nadal, G. Perry, and D. Tanre, "Remote sensing of aerosols over land surfaces from POLDER-ADEOS-1 polarized measurements," *J. Geophys. Res. - Atmos.* **106**(D5), 4913–4926 (2001).
26. M. Herman, J. L. Deuze, A. Marchand, B. Roger, and P. Lallart, "Aerosol remote sensing from POLDER/ADEOS over the ocean: improved retrieval using a nonspherical particle model," *J. Geophys. Res. - Atmos.* **110**(D10), D10S02 (2005).
27. O. Hagolle, P. Goloub, P. Y. Deschamps, H. Cosnefroy, X. Briottet, T. Bailleul, J. M. Nicolas, F. Parol, B. Lafrance, and M. Herman, "Results of POLDER in-flight calibration," *IEEE Trans. Geosci. Remote Sensing* **37**(3), 1550–1566 (1999).
28. B. Fougnie, G. Bracco, B. Lafrance, C. Ruffel, O. Hagolle, and C. Tinel, "PARASOL in-flight calibration and performance," *Appl. Opt.* **46**(22), 5435–5451 (2007).
29. C. Cox and W. Munk, *Slopes of the Sea Surface Deduced from Photographs of Sun Glitter*, C. Cox and W. Munk, eds. (Scripps Institution of Oceanography, 1956).
30. G. G. Stokes, "On the composition and resolution of streams of polarized light from different sources," *Trans. Cambridge Philos. Soc.* **3**, 233–259 (1852).
31. M. I. Mishchenko, L. D. Travis, and A. A. Lacis, *Multiple scattering of light by particles: Radiative transfer and coherent backscattering* (Cambridge Univ. Press, New York, 2006).
32. M. I. Mishchenko, "The 3*3 approximation in the CP representation of the Stokes vector in polarized-radiation transport in planetary atmospheres," *Kinematics Phys. Celestial Bodies* **3**, 29–34 (1987).
33. K. L. Coulson, *Polarization and Intensity of Light in the Atmosphere* (A. Deepak Pub., Hampton, Va., USA, 1988).

34. J. E. Hansen, "Multiple scattering of polarized light in planetary atmospheres part II. Sunlight reflected by terrestrial water clouds," *J. Atmos. Sci.* **28**(8), 1400–1426 (1971).
35. Y. Kawata, "Circular polarization of sunlight reflected by planetary atmospheres," *Icarus* **33**(1), 217–232 (1978).
36. S. Y. Kotchenova, E. F. Vermote, R. Matarrese, and F. J. Klemm, Jr., "Validation of a vector version of the 6S radiative transfer code for atmospheric correction of satellite data. Part I: path radiance," *Appl. Opt.* **45**(26), 6762–6774 (2006).
37. J. W. Hovenier, "A unified treatment of polarized light emerging from a homogeneous plane-parallel atmosphere," *Astron. Astrophys.* **183**, 363–370 (1987).
38. H. C. van de Hulst, *Light Scattering by Small Particles* (Wiley, New York, 1957).
39. M. Chami, R. Santer, and E. Dilligeard, "Radiative transfer model for the computation of radiance and polarization in an ocean-atmosphere system: polarization properties of suspended matter for remote sensing," *Appl. Opt.* **40**(15), 2398–2416 (2001).
40. J. L. Deuzé, M. Herman, and R. Santer, "Fourier-Series Expansion Of The Transfer Equation In The Atmosphere Ocean System," *J. Quant. Spectrosc. Radiat. Transf.* **41**(6), 483–494 (1989).
41. K. Ding and H. R. Gordon, "Atmospheric correction of ocean-color sensors: effects of the Earth's curvature," *Appl. Opt.* **33**(30), 7096–7106 (1994).
42. C. N. Adams and G. W. Kattawar, "Radiative transfer in spherical shell atmospheres: I. Rayleigh scattering," *Icarus* **35**(1), 139–151 (1978).
43. M. Wang, "Light scattering from the spherical-shell atmosphere: earth curvature effects measured by SeaWiFS," *Eos Trans. AGU* **84**(48), 529–534 (2003).
44. Y. Kawata, A. Yamazaki, T. Kusaka, and S. Ueno, "Aerosol retrieval from airborne Polder data by multiple scattering model," presented at *IGARSS, Surface and Atmospheric Remote Sensing*, (1994), 1895–1897.
45. J. W. Strutt, Lord Rayleigh, "On the light from the sky, its polarisation and colour. II," *Philos. Mag.* **41**, 274–279 (1871).
46. J. L. Deuze, "Etude de la polarisation du rayonnement par les milieux diffusants: application à la polarisation localisée de Vénus," PhD dissertation (Université des sciences et technique de Lille, France, 1974).
47. IOCCG, *Remote sensing of inherent optical properties: fundamentals, tests of algorithms, and applications*, Z. P. Lee, ed., Reports of the International Ocean Colour Coordinating Group No. 5, (2006).
48. E. F. Vermote and A. Vermeulen, *Atmospheric Correction Algorithm: Spectral Reflectances (MOD09)*, E. F. Vermote and A. Vermeulen, eds., 4.0 (US National Aeronautics and Space Administration, 1999).
49. A. Morel, "Optical properties of pure water and pure seawater," in *Optical Aspects of Oceanography*, N. G. Jerlov and E. S. Nielsen, eds. (Academic, New York, 1974), pp. 1–24.
50. R. M. Pope and E. S. Fry, "Absorption spectrum (380–700 nm) of pure water. 2. Integrating cavity measurements," *Appl. Opt.* **36**(33), 8710–8723 (1997).
51. A. Bricaud, A. Morel, M. Babin, K. Allali, and H. Claustre, "Variations of light absorption by suspended particles with chlorophyll a concentration in oceanic (case 1) waters: analysis and implications for bio-optical models," *J. Geophys. Res.* **103**(C13), 31033–31044 (1998).
52. H. Loisel and A. Morel, "Light scattering and chlorophyll concentration in case 1 waters: A reexamination," *Limnol. Oceanogr.* **43**(5), 847–858 (1998).
53. H. Bader, "Hyperbolic distribution of particle sizes," *J. Geophys. Res.* **75**(15), 2822–2830 (1970).
54. A. Morel, "Are the empirical relationships describing the bio-optical properties of case 1 waters consistent and internally compatible?" *J. Geophys. Res.* **114**(C1), C01016 (2009).
55. D. Stramski, E. Boss, D. Bogucki, and K. J. Voss, "The role of seawater constituents in light backscattering in the ocean," *Prog. Oceanogr.* **61**(1), 27–56 (2004).
56. D. Stramski, A. Bricaud, and A. Morel, "Modeling the inherent optical properties of the ocean based on the detailed composition of the planktonic community," *Appl. Opt.* **40**(18), 2929–2945 (2001).
57. K. J. Voss and E. S. Fry, "Measurement of the Mueller Matrix for Ocean Water," *Appl. Opt.* **23**(23), 4427–4439 (1984).
58. K. T. Whitby, "The physical characteristics of sulfur aerosols," *Atmos. Environ.* **12**(1-3), 135–159 (1978).
59. C. Junge, "The size distribution and aging of natural aerosols as determined from electrical and optical data on the atmosphere," *J. Atmos. Sci.* **12**, 13–25 (1955).
60. C. E. Junge, *Air Chemistry and Radioactivity*, International Geophysics (Academic, New York, 1963).
61. Y. J. Kaufman, A. Smirnov, B. N. Holben, and O. Dubovik, "Baseline maritime aerosol: methodology to derive the optical thickness and scattering properties," *Geophys. Res. Lett.* **28**(17), 3251–3256 (2001).
62. P. N. Francis, P. Hignett, and J. P. Taylor, "Aircraft observations and modeling of sky radiance distributions from aerosol during TARFOX," *J. Geophys. Res.* **104**(D2), 2309–2319 (1999).
63. O. Dubovik, A. Smirnov, B. N. Holben, M. D. King, Y. J. Kaufman, T. F. Eck, and I. Slutsker, "Accuracy assessments of aerosol optical properties retrieved from Aerosol Robotic Network (AERONET) Sun and sky radiance measurements," *J. Geophys. Res.* **105**(D8), 9791–9806 (2000).
64. J. L. Deuzé, P. Goloub, M. Herman, A. Marchand, G. Perry, S. Susana, and D. Tanre, "Estimate of the aerosol properties over the ocean with POLDER," *J. Geophys. Res. - Atmos.* **105**(D12), 15329–15346 (2000).

65. I. Veselovskii, A. Kolgotin, V. Griaznov, D. Müller, K. Franke, and D. N. Whiteman, "Inversion of multiwavelength Raman lidar data for retrieval of bimodal aerosol size distribution," *Appl. Opt.* **43**(5), 1180–1195 (2004).
66. O. Dubovik, B. Holben, T. F. Eck, A. Smirnov, Y. J. Kaufman, M. D. King, D. Tanré, and I. Slutsker, "Variability of absorption and optical properties of key aerosol types observed in worldwide locations," *J. Atmos. Sci.* **59**(3), 590–608 (2002).
67. M. I. Mishchenko, L. D. Travis, R. A. Kahn, and R. A. West, "Modeling phase functions for dustlike tropospheric aerosols using a shape mixture of randomly oriented polydisperse spheroids," *J. Geophys. Res.* **102**(D14), 16831–16847 (1997).
68. M. I. Mishchenko, J. W. Hovenier, and L. D. Travis, *Light Scattering by Nonspherical Particles: Theory, Measurements, and Applications* (Academic, San Diego, 2000), p. 690.
69. H. Volten, O. Munoz, E. Rol, J. F. de Haan, W. Vassen, J. W. Hovenier, K. Muinonen, and T. Nousiainen, "Scattering matrices of mineral aerosol particles at 441.6 nm and 632.8 nm," *J. Geophys. Res.- Atmos.* **106**(D15), 17375–17401 (2001).
70. M. Wang and H. R. Gordon, "Radiance reflected from the ocean-atmosphere system: synthesis from individual components of the aerosol size distribution," *Appl. Opt.* **33**(30), 7088–7095 (1994).
71. D. Tanré, Y. J. Kaufman, M. Herman, and S. Mattoo, "Remote sensing of aerosol properties over oceans using the MODIS/EOS spectral radiances," *J. Geophys. Res.- Atmos.* **102**(D14), 16971–16988 (1997).
72. R. C. Levy, L. A. Remer, D. Tanré, S. Mattoo, and Y. J. Kaufman, *Algorithm for remote sensing of tropospheric aerosol over dark targets from MODIS*, R. C. Levy, L. A. Remer, D. Tanré, S. Mattoo, and Y. J. Kaufman, eds., Collections 005 and 051: Revision 2 (2009).
73. A. Ångström, "On the Atmospheric Transmission of Sun Radiation and on Dust in the Air," *Geogr. Ann.* **11**, 156–166 (1929).
74. G. L. Schuster, O. Dubovik, and B. N. Holben, "Angstrom exponent and bimodal aerosol size distributions," *J. Geophys. Res.* **111**, D07207 (2006).
75. A. Smirnov, B. N. Holben, Y. J. Kaufman, O. Dubovik, T. F. Eck, I. Slutsker, C. Pietras, and R. N. Halthore, "Optical Properties of Atmospheric Aerosol in Maritime Environments," *J. Atmos. Sci.* **59**(3), 501–523 (2002).
76. T. F. Eck, B. N. Holben, J. S. Reid, O. Dubovik, A. Smirnov, N. T. O'Neill, I. Slutsker, and S. Kinne, "Wavelength dependence of the optical depth of biomass burning, urban, and desert dust aerosols," *J. Geophys. Res.* **104**(D24), 31333–31349 (1999).
77. M. D. King and D. M. Byrne, "A Method for Inferring Total Ozone Content from the Spectral Variation of Total Optical Depth Obtained with a Solar Radiometer," *J. Atmos. Sci.* **33**(11), 2242–2251 (1976).
78. N. T. O'Neill, T. F. Eck, A. Smirnov, B. N. Holben, and S. Thulasiraman, "Spectral discrimination of coarse and fine mode optical depth," *J. Geophys. Res.* **108**(D17), 4559 (2003).
79. E. Boesche, P. Stammes, T. Ruhtz, R. Preusker, and J. Fischer, "Effect of aerosol microphysical properties on polarization of skylight: sensitivity study and measurements," *Appl. Opt.* **45**(34), 8790–8805 (2006).
80. O. Hagolle, A. Guerry, L. Cunin, B. Millet, J. Perbos, J. M. Laherrere, T. Bret-Dibat, and L. Poutier, "POLDER level 1 processing algorithms," *Proc. SPIE* **2758**, 308–319 (1996).
81. K. D. Moore, K. J. Voss, and H. R. Gordon, "Spectral reflectance of whitecaps: Their contribution to water-leaving radiance," *J. Geophys. Res.* **105**(C3), 6493–6499 (2000).
82. R. Frouin, M. Schwindling, and P.-Y. Deschamps, "Spectral reflectance of sea foam in the visible and near-infrared: In situ measurements and remote sensing implications," *J. Geophys. Res.* **101**(C6), 14,361–314,371 (1996).
83. R. E. Eplee, W. D. Robinson, S. W. Bailey, D. K. Clark, P. J. Werdell, M. Wang, R. A. Barnes, and C. R. McClain, "Calibration of SeaWiFS. II. Vicarious techniques," *Appl. Opt.* **40**(36), 6701–6718 (2001).
84. T. Harmel, "Apport des mesures directionnelles et polarisées aux corrections atmosphériques au-dessus des océans ouverts. Application à la mission PARASOL," Thèse (l'Université P. & M. Curie, Paris, 2009).
85. IOCCG, *Minimum requirements for an operational, ocean-colour sensor for the open ocean*, A. Morel, ed., Reports of the International Ocean Colour Coordinating Group No. 1 (IOCCG, 1997).
86. J. E. O'Reilly, S. Maritorena, G. Mitchell, D. A. Siegel, K. L. Carder, D. L. Garver, M. Kahru, and C. R. McClain, "Ocean color chlorophyll algorithms for Seawifs," *J. Geophys. Res.* **103**(C11), 24937–24953 (1998).
87. E. Bosc, A. Bricaud, and D. Antoine, "Seasonal and interannual variability in algal biomass and primary production in the Mediterranean Sea, as derived from 4 years of SeaWiFS observations," *Global Biogeochem. Cycles* **18**(1), GB1005 (2004).
88. B. N. Holben, T. F. Eck, I. Slutsker, D. Tanre, J. P. Buis, A. Setzer, E. Vermote, J. A. Reagan, Y. J. Kaufman, T. Nakajima, F. Lavenu, I. Jankowiak, and A. Smirnov, "AERONET-A Federated Instrument Network and Data Archive for Aerosol Characterization," *Remote Sens. Environ.* **66**(1), 1–16 (1998).
89. D. K. Clark, H. R. Gordon, K. J. Voss, Y. Ge, W. Broenkow, and C. Trees, "Validation of atmospheric correction over the oceans," *J. Geophys. Res.* **102**(D14), 17209–17217 (1997).

1. Introduction

The recent progress made in the field of ocean color radiometry (OCR) sensing allowed to increase the diversification of satellite derived biogeophysical products such as the phytoplankton functional types product [1] and the water transparency product [2]. The chlorophyll concentration retrieved from the satellite imagery is now assimilated into ecological or climatic models [3] and some studies use these data to commensurate the oceanic impact of the global change [4–6]. However, all those refinements primarily rely on the radiometric accuracy of the atmospheric correction processing.

The main goal of atmospheric correction over open ocean is to remove the atmospheric and sea surface effects from satellite observations in order to retrieve the water-leaving radiance. The atmospheric correction step is highly important in ocean color remote sensing because of the weak contribution of the water leaving radiance to top of atmosphere (TOA) signal relatively to atmospheric component [7]. In the last decades, numerous OCR satellite missions have been successfully launched such as, to mention only a few, the Sea-Viewing Wide Field-of-View Sensor (SeaWiFS/NASA), Moderate Resolution Imaging Spectroradiometer (MODIS/NASA), Medium Resolution Imaging Spectrometer (MERIS/ESA), Polarization and Directionality of the Earth's Reflectances (POLDER/CNES). Note that the third generation of POLDER sensor (POLDER 3 on PARASOL satellite) is currently the sole sensor which is able to provide multidirectional and polarized measurements over the oceans from space.

In the visible part of the spectrum, the atmospheric radiance, along with its component reflected on the sea surface, corresponds to more than 90% of the measured TOA radiance. Those two components need to be accurately estimated by the atmospheric correction procedure in order to retrieve the water-leaving radiance. Moreover, this atmospheric radiance is highly variable due to the high spatiotemporal variability of the optical properties of aerosols [8]. Therefore, the development of even more accurate atmospheric correction algorithms remains a challenging task. The application of atmospheric correction algorithms to satellite data provides aerosol optical property retrievals whose accuracy can also be significantly improved [9]. Current atmospheric correction procedures rely on the fact that the water-leaving radiance can be assumed negligible in the red and infrared spectral bands because of the high absorption coefficient of seawater. Thus, the signal measured by a satellite sensor at these wavelengths carries information on the atmosphere layer only and can be used to estimate the aerosol optical properties [10–13]. Based on these derived optical properties, the atmospheric signal is extrapolated from the red to the shorter wavelengths (i.e., visible bands). However, such an extrapolation might lead to significant uncertainties in the retrieved water leaving radiances because of a wrong assessment of atmospheric optical properties at the visible wavelengths. Recent studies, based on comparison of satellite and in situ data, demonstrated the need to improve performances of the atmospheric correction algorithms over open ocean and coastal waters [14–16].

Previous works showed that the satellite polarized radiance is nearly insensitive to variations in phytoplankton concentration in open ocean waters both in the near-infrared and the blue/green part of the spectrum [17–19]. This is mainly because polarization by molecular Rayleigh scattering dominates the signal which reaches the top of atmosphere. Nevertheless, on the basis of a large set of PARASOL data, it has been shown that the impact of the variations in phytoplankton concentration on the PARASOL Rayleigh-corrected top-of-atmosphere measurements remains negligible relative to the radiometric accuracy of PARASOL sensor [18]. As a result, the polarization signal measured over the open ocean at the top of atmosphere can be used to characterize the optical properties of the atmosphere regardless of the optical characteristics of the observed water mass. Therefore, there is room for improvement in terms of performance for retrieval of the oceanic optical properties from space. Furthermore, several studies [19–22] have highlighted that the remote sensing algorithms for aerosol detection which use both scalar radiance and polarization measurements are less dependent on *a priori* information used to constrain the retrieval

algorithm than those which make use of the scalar radiance measurements only. As a result of these studies, the polarization measurements can be satisfactorily used to retrieve the aerosol optical thickness, aerosol effective radius, and aerosol refractive index.

The exploitation of the polarimetric data has recently been reported as one of the main perspectives of the aerosol detection from space [23]. To our knowledge, the TOA polarized information has never been exploited to derive water leaving radiances for ocean color purposes. An atmospheric correction algorithm has been developed to retrieve the water-leaving radiances and the aerosol characteristics simultaneously. Such an algorithm is currently dedicated to the sole satellite sensor measuring the multidirectional polarized radiance (POLDER 3 on PARASOL, hereafter referred to as "PARASOL"). Note that the algorithm could be potentially adjusted to the future NASA mission Aerosols, Clouds and Ecosystems (ACE) and its preparatory mission (PACE) which is scheduled for launch around 2018 and will carry a multidirectional polarimeter instrument.

This paper is organized as follows. Since only a few studies were devoted in the past to use PARASOL data for ocean color analysis, the main characteristics of the multidirectional and polarimetric data of such a sensor are first briefly described. Then, an original polarization-based atmospheric correction algorithm is proposed. The impact of the multidirectional information to retrieve aerosol properties and water-leaving radiance retrieval is discussed as well. The third part of the paper deals with the analysis of the influence of the polarized information of the visible bands on the determination of aerosol type. At last, the proposed polarization-based atmospheric correction algorithm is applied to PARASOL satellite images and the importance of the polarimetric satellite data for atmospheric correction over open ocean waters is discussed.

2. PARASOL features

PARASOL sensor (French space agency, *Centre National d'Etudes Spatiales*, CNES) is primarily dedicated to improve knowledge of the radiative and microphysical properties of clouds and aerosols by measuring the intensity and the polarization state of light in several different viewing directions. PARASOL sensor is the third generation of the POLDER (Polarization and Directionality of the Earth Reflectances) instrument [24–26]. The optical device of PARASOL is characterized by a wide field of view ($\sim 114^\circ$). A CCD matrix array detector (242*274 elements) allows acquiring two-dimensional pictures of the Earth [24]. The nadir pixel size is about 6 km per 7 km.

One of the main features of interest of PARASOL is its ability to observe a given ground target at different viewing angles (up to 16 viewing angles) along the satellite track. Therefore, a part of the bidirectional reflectance distribution function of a target is measured with PARASOL. The total acquisition time for a whole multidirectional sequence is performed within a 4-minute time window for which the geophysical parameters of the scene can be assumed as virtually similar [24]. The Stokes parameter I , which corresponds to the top-of-atmosphere radiance, is measured at nine wavelengths ranging from 443 to 1020 nm. In addition, three wavelengths channels, namely 490 nm, 670 nm and 865 nm, are equipped with polarizers thus allowing the measurement of the Stokes parameters Q and U which are informative on the linear degree and the plane of polarization. The TOA radiances are normalized as follows: the Stokes parameters are multiplied by π/E_λ , where E_λ is the extraterrestrial solar irradiance [27]. The normalized radiances are thus unitless. The ratio between the radiances and the cosine of the solar zenith angle allows getting reflectance values. The noise equivalent normalized radiance of PARASOL data is about $4 \cdot 10^{-4}$ [28]. Note that the viewing geometries of PARASOL pixels for which the sun glint radiance, as computed using Cox and Munk model [29] for a wind speed of 4 m s^{-1} , is higher than PARASOL noise are ignored in the current study.

3. Multi-directionality and POLarization-based Atmospheric Correction algorithm (POLAC algorithm)

3.1. Algorithm overview

Recent studies showed that the polarized signal at the top of atmosphere, in particular in the visible part of the spectrum such as 490 nm, is fairly insensitive to the variations of the water-constituents concentrations in open ocean conditions and thus exploitable for atmospheric correction purposes over those areas [17, 18]. However, the use of the polarized signal, especially at the shorter wavelengths of the visible spectrum, has never been implemented, to our knowledge, to retrieve the aerosol optical properties together with the water-leaving radiances. A specific atmospheric correction algorithm, so-called *multi-directionality and POLarization-based Atmospheric Correction* (hereafter referred to as POLAC), was therefore developed based on the multidirectional and polarized data of PARASOL sensor. This section provides a general overview of POLAC algorithm.

POLAC algorithm is composed of two principal phases, hereafter noted phase (P1) and (P2): (P1) and (P2) deals with the retrieval of the aerosol optical properties and the water-leaving radiance respectively (Fig. 1). The two phases make use of an optimization scheme which is performed to retrieve the geophysical parameters of interest. The optimization process is achieved between PARASOL measurements and simulations carried out using a vector radiative transfer model which was designed for simulating the light field including polarization in the atmosphere-ocean system. The optical properties of the aerosols are determined based on the radiance (i.e. Stokes parameter I) in the near-infrared (NIR), namely at 865 nm, as well as the Stokes parameters Q and U in the visible spectrum and NIR as measured by PARASOL, namely at Q and U at 490, 670 and 865 nm. Note that Q and U are supposed to be insensitive to the variations of the in-water-constituent concentrations [17, 18]. The phase (P1) is subdivided into two iterative steps; Q and U are primarily used in a first step for retrieving the best bimodal aerosol model. A bimodal aerosol model is defined as a couple of a fine mode and a coarse mode as well as their respective proportion. In a second step, the scalar radiance I is used to derive the aerosol optical thickness. The convergence of the iterative procedure is typically obtained after two or three iterations. Based on the retrieved values of aerosol optical properties, the phase (P2) is activated to derive the water-leaving radiance in the visible spectrum (i.e. PARASOL bands centered on 490, 565, 670 nm). The water leaving radiance is retrieved by matching the measurements of scalar TOA radiance with radiative transfer simulations computed for various hydrosol compositions of

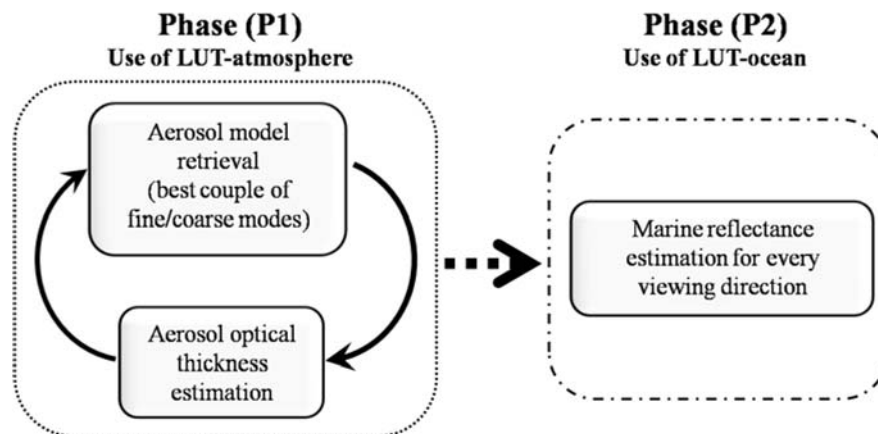


Fig. 1. Overview of the so-called multi-directionality and POLarization-based Atmospheric Correction (POLAC) algorithm.

the oceanic layer. Such a procedure is carried out for each observation geometry of a given PARASOL pixel.

3.2. Modeling approach

3.2.1. Radiative transfer in a coupled atmosphere-ocean system

A beam light of arbitrary polarization can be represented by the Stokes vector $\mathbf{S} = (I, Q, U, V)^T$, the superscript T stands for the transpose of the vector [30, 31]. The first Stokes parameter, I , describes the total (sum of polarized and unpolarized) radiance. The next two terms, Q and U , describe the linearly polarized radiance, and the last one, V , stands for the circularly polarized radiance. The importance of the latter is commonly assumed negligible in comparison to the others at the top of atmosphere [32–36]. The radiative transfer equation in a medium governed by absorption and scattering mechanisms can be written at a given wavelength as follows:

$$\mu \frac{d\mathbf{S}(\tau, \mu, \phi)}{d\tau} = \mathbf{S}(\tau, \mu, \phi) - \frac{\omega(\tau)}{4\pi} \iint_{\Omega} \mathbf{P}(\mu, \phi, \mu', \phi') \mathbf{S}(\tau, \mu', \phi') d\mu' d\phi', \quad (1)$$

where τ is the optical thickness of the medium; μ and ϕ are the cosine of the viewing angle and the azimuth angle, respectively. The superscript prime denotes the incident direction. By convention the relative azimuth $\Delta\phi$ is equal to 180° when the Sun and the sensor are in opposition. The second term of the right-hand side of (1), called the source term, depends explicitly on the phase matrix \mathbf{P} and the single scattering albedo ω . The phase matrix \mathbf{P} is obtained by rotating the so-called scattering matrix \mathbf{F} from the viewing plane to the scattering plane. The scattering matrix of aerosols or hydrosols can be written for a given scattering angle Θ as follows [37, 38]:

$$\mathbf{F}(\Theta) = \begin{pmatrix} F_{11}(\Theta) & F_{12}(\Theta) & 0 & 0 \\ F_{12}(\Theta) & F_{22}(\Theta) & 0 & 0 \\ 0 & 0 & F_{33}(\Theta) & F_{34}(\Theta) \\ 0 & 0 & -F_{34}(\Theta) & F_{44}(\Theta) \end{pmatrix}, \quad (2)$$

In this study, the OSOA model [39] was used to solve numerically the vector radiative transfer equation for the coupled atmosphere-ocean system. This model is based on the successive orders of scattering method [40]. The atmosphere and the ocean are assumed plane-parallel. Such an assumption is valid for solar zenith angles smaller than 70° [41–43]. The ocean surface is assumed flat. It has been shown that the effect of waves on the polarized signal measured at the top of atmosphere is weak [44]. The use of the polarized information in our atmospheric correction algorithm thus makes sense. The optical properties of the molecular component of the radiation are known for both atmospheric and oceanic cases and are given by Rayleigh's formulation [45]. The vertical distributions of molecules and aerosols are modeled as exponentially decreasing with respect to the height with 8-km and 2-km scale heights for molecules and aerosols, respectively. The atmosphere is divided into 26 layers to account for the vertical inhomogeneity, in accordance with the sensitivity studies performed by Deuzé [46]. Based on the sensitivity studies performed by Chami et al. [39], the ocean is numerically discretized into 80 layers to account for the vertical inhomogeneity. Here, the vertical profile of the oceanic constituents is assumed to be homogeneously distributed [47]. The Stokes parameters measured from the satellite are first corrected from the effects of gaseous absorption (these effects are estimated using the 6S radiative transfer model [48]) prior to their comparison with the OSOA simulations.

3.2.2. Oceanic models

In the OSOA model, the oceanic layer is usually described using a seawater model comprising four components which are pure seawater, phytoplankton pigments and their by-products, inorganic suspended material and colored dissolved organic matter. Since this study focuses on the analysis of signal variations over phytoplankton-dominated water type, only pure seawater, phytoplankton and its co-varying particles components are considered here. The inherent optical properties of these components are modeled as follows. The scattering and absorption coefficients of pure seawater are taken from Morel [49] and Pope and Fry [50] respectively. The absorption coefficient of phytoplankton and co-varying particles is derived from the bio-optical model of Bricaud et al. [51]. The phytoplankton scattering coefficient is modeled as suggested by Loisel and Morel [52]. The bulk refractive index of phytoplankton relative to water is 1.05. The size distribution of phytoplankton cells is assumed to follow the Junge hyperbolic distribution, which is commonly used for oceanic environment [53, 54], with Junge exponent values of -4.5 , -4 , -3.5 .

The scattering matrix of phytoplankton, which contains the information on its total and polarized phase function, is computed by means of Mie theory [55]. It has been argued that reasonable fits to the phase function (F_{11} term of the scattering matrix) can be obtained using Mie theory [56]. In addition, the other non-null elements of the scattering matrix, which govern the polarized components of light, are calculated here using realistic input parameters for phytoplankton that leads to values close to the Rayleigh approximation of pure sea water. Therefore, the simulated polarization features of phytoplankton are in agreement with what has been found for natural oceanic water samples [18, 57] and thus, making our computations meaningful.

3.2.3. Aerosol models

Aerosols determination by remote sensing techniques relies primarily on the aerosol models used, which should be as representative as possible of their worldwide climatology. As pointed out by Whitby [58] and Junge [59, 60], a realistic size distribution can be modeled based on the sum of single modes. Several studies showed that a satisfactory simulation of aerosols can be obtained using a mixture of a fine mode with a coarse mode [61–65]. The size distribution $N(r)$ of these two modes can be parameterized with the same log-normal expression, as follows:

$$dN_i(r) = \frac{1}{\sigma_i \sqrt{2\pi}} \exp \left[-\frac{1}{2} \left(\frac{\log r - \log \bar{r}_i}{\sigma_i} \right)^2 \right] d \log r, \quad (3)$$

where \bar{r}_i , the mean radius, and σ_i , the standard deviation of $\log r$, are specific for the given mode i . The application of Eq. (3) into the Mie theory calculations leads to the aerosol scattering matrix $F(\Theta)$, which has the following characteristics: $F_{11}(\Theta) = F_{22}(\Theta)$ and $F_{33}(\Theta) = F_{44}(\Theta)$, the upper left element $F_{11}(\Theta)$ is the so-called phase function. Since the Stokes parameter V could be neglected for atmospheric applications [30], only three elements are necessary to characterize the aerosol single scattering, $F_{11}(\Theta)$, $F_{12}(\Theta)$ and $F_{33}(\Theta)$. The scattering matrix of each aerosol mode was used as an input of the OSOA model to generate the LUTs. The optical properties of aerosols used in this study are listed in Table 1. These values were provided by the *Laboratoire d'Optique Atmospherique* (Université de Lille, France) based on the results derived by Dubovik et al. [66] from AERONET network observations. It has been shown that the representativeness of the aerosol climatology is strongly strengthened by the use of non-spherical aerosol models [26, 64, 67]. The phase matrix of such aerosol types can be calculated for various shapes by the T-matrix theory [67, 68] for small aerosol particles or can be measured in the laboratory. In this study, the non-

spherical aerosol model measured by Volten et al. [69] is used. Note that this model is assumed to be spectrally flat.

Table 1. Microphysical properties of the fine and coarse modes of the spherical aerosol models used to construct the LUT*

<i>Fine modes</i>			<i>Coarse modes</i>		
\bar{r}_i	<i>Refractive index</i>	σ_i	\bar{r}_i	<i>Refractive index</i>	σ_i
0.04, 0.08, 0.10, 0.13	1.35, 1.45, 1.60	0.2	0.75	1.33, 1.35, 1.37	0.304

*The mean radius, \bar{r}_i , and the standard deviation, σ_i , are given in μm . Only non-absorbing aerosols, for which the imaginary part of the refractive index is equal to 0, were considered in this study. Note that the microphysical properties of the non-spherical coarse mode are not indicated in this table since its optical properties were directly obtained from laboratory measurements by Volten et al. [69].

For each of the fine and coarse modes, simulations have been generated and stored in look-up tables (LUT) for optical thicknesses $\tau(\lambda = 550\text{nm})$ ranging from 0 (purely molecular atmosphere) to 1 (very turbid atmosphere). On the one hand, the Stokes parameters I , Q and U at the top of atmosphere, calculated for a Chlorophyll-a concentration (Chl) value of 0.03 mg m^{-3} , have been stored in the so-called LUT-atmosphere for the wavelengths which are insensitive to Chl variations, namely in the red-infrared part of spectrum (for I , Q , U) and in the visible (for Q , U only). On the other hand, the so-called LUT-ocean were constructed by storing the simulated Stokes parameter I at the top of atmosphere, as well as I just beneath the sea surface, for different oceanic models with Chl values ranging from 0.03 to 30 mg m^{-3} .

3.3. Inversion scheme

The POLAC inversion scheme is based on the minimization of the Euclidian distance between the measured directional data and simulations of the radiative transfer model. At each step of the algorithm, the variables which need to be retrieved (e.g. aerosol optical thickness, fine mode, water-leaving radiance...) are represented as a vector, denoted \mathbf{x} . A mono-directional and multi-directional cost functions are defined with respect to \mathbf{x} to take into account the different dynamics exhibited by the values of the three Stokes parameters acquired at different wavelengths and viewing geometries. The cost function J is defined for a given viewing geometry configuration, denoted Ψ , as follows:

$$J(\Psi, \mathbf{x}) = \sum_i^{N_{cri}} p_i(\Psi) \frac{(S_i^{mes}(\Psi) - S_i^{sim}(\Psi, \mathbf{x}))^2}{\sigma_i^2(\Psi)} \quad (4)$$

where N_{cri} is the number of criteria used in the retrieval procedure; here a criterion is defined as one of the Stokes parameters I , Q or U for a given wavelength. S_i^{mes} and S_i^{sim} stand for the measured and simulated value of the i^{th} criterion, respectively. The parameter σ_i is the absolute uncertainty affecting the measurement of S_i^{mes} ; here σ_i is taken as the noise equivalent normalized radiance as calculated by [28]. It should be noted that σ_i is used as a normalization factor which takes into account the uncertainty of each satellite measurement. Finally, the p_i is the variance of S_i^{sim} calculated over the entire set of \mathbf{x} used in the simulations, more explicitly p_i is calculated for a given viewing geometry as follows:

$$p_i = \frac{1}{N_{LUT} - 1} \sum_{j=1}^{N_{LUT}} (S_i^{sim}(\mathbf{x}_j) - \langle S_i^{sim} \rangle)^2 \quad (5)$$

where N_{LUT} is the total number of values taken by \mathbf{x} in the look-up tables generation and $\langle S_i^{sim} \rangle$ is the average of the simulated S_i over the set of \mathbf{x}_j . The p factor is an estimator of the amount of information contained in a given Stokes parameter that is effectively used to retrieve the desired variable \mathbf{x} . In other words, the greater p is, the more informative S is.

The multi-directional cost function J^* is then given by:

$$J^*(\mathbf{x}) = \sum_k^{N_{dir}} J(\Psi_k, \mathbf{x}) \quad (6)$$

where N_{dir} is the number of viewing configurations available. In the algorithm, the values of the vector \mathbf{x} are obtained after minimization of the appropriate cost function, either J or J^* . It should be noted that the use of such cost functions could lead to ambiguities in the retrieval scheme (i.e. various solutions could lead to the same minimum cost function). The impact of such ambiguities on the retrievals made by the POLAC algorithm and the subsequent solutions to reduce this impact are addressed in section 4.

3.3.1. Aerosol optical thickness estimation

The computation of the aerosol optical thickness, τ_a , proceeds by minimization of the cost function generated using the criterion $S = I(865\text{nm})$. Here, $\mathbf{x} = \{\tau_a(550\text{nm})\}$. The mono- or multi-directional cost function (J or J^* , respectively) is calculated for each τ_a values stored in the LUT-atmosphere and for a given aerosol model. Hereafter, the use of J or J^* will be referred to as *mono-* or *multi-directional* approach, respectively. Minimization of J enables to compute τ_a for each viewing configuration separately, whereas minimization of J^* merges the directional information. Then, based on the method of least squares, a polynomial function f is used to fit the numerical values of J or J^* such as $J^* = f(\tau_a)$. A satisfactory fitting is obtained by using a second degree polynomial as follows:

$$J(\tau_a) \text{ or } J^*(\tau_a) = A + B\tau_a + C\tau_a^2. \quad (7)$$

The aerosol optical thickness is then straightforwardly retrieved by solving that polynomial.

During this step of the algorithm in which τ_a is estimated, the TOA radiance is simulated for a given aerosol model to compute the cost function. However, the aerosol phase matrix is a function of the viewing geometry and, subsequently, different aerosol types induce different directional distributions of the TOA radiance for the same optical thickness. Therefore, the use of a wrong aerosol model to estimate τ_a might provide wrong outcomes depending on the directional approach used. In the following, the mono- and multi-directional approaches for estimating τ_a are compared to determine the approach which is the least disrupted by the choice of the aerosol model.

Let us consider τ_a^* and $\tau_{a,dir}$ the aerosol optical thickness estimated by the multi-directional approach (i.e. minimization of J^*) and the mono-directional approach (i.e. minimization of J), respectively. Three procedures are compared to estimate the aerosol optical thickness τ_a based on: (i) the multidirectional approach (noted as τ_a^*), (ii) the average value of $\tau_{a,dir}$ over the entire set of viewing configurations retrieved with the mono-directional approach, (iii) the median value of $\tau_{a,dir}$ retrieved with the mono-directional approach. Those three procedures were applied to a large set of synthetic data simulated by OSOA model for representative amounts and models of aerosols. First, the TOA radiance at 865 nm was simulated for various values of τ_a and for all the aerosol models stored in the LUT-atmosphere to consider a great number of PARASOL-like synthetic data. Second, the three τ_a estimation procedures are applied to those synthetic data. The aerosol model used in those procedures was set to the non-spherical model. The procedures (i), (ii) and (iii) are then applied to the synthetic data simulated for all the aerosol models of the LUT used in this

study so that the sensitivity of each procedure to those models is evaluated. The less sensitive is the procedure to the aerosol models, the faster the convergence is reached between the two steps of the phase (P1) of the algorithm and finally the more accurate the aerosol parameter retrieval is.

The three procedures were applied to the entire set of viewing configurations encountered in actual PARASOL images (Fig. 2). In the three cases, the estimate of τ_a (i.e. τ_a^* , average of $\tau_{a,dir}$, median of $\tau_{a,dir}$) is highly correlated to the desired optical thickness (correlation coefficient >0.99). The slopes of the regression are close to the 1:1 line within 10%. However, a slight underestimation of τ_a is observed. The τ_a^* values are the most scattered around the regression line. The absolute percentage difference (APD) and the absolute difference (AD) are used in the rest of the article in order to statistically estimate the accuracy of the retrievals. These variables are defined as follows:

$$APD = \frac{1}{N} \sum_{i=1}^N \frac{|y_i - x_i|}{x_i} \quad (8)$$

$$AD = \frac{1}{N} \sum_{i=1}^N |y_i - x_i| \quad (9)$$

where x_i and y_i stand for the desired and the retrieved values, respectively. N is the total number of retrievals. The APD value is 15% for such case (procedure (i)), whereas the APD is reduced to 8.3% for the procedure (ii) and less than 7.5% for the procedure (iii). The latter exhibits the best robustness. Therefore, this procedure has been implemented into the POLAC algorithm. Furthermore, the set of $\tau_{a,dir}$ obtained for each pixel enables to compute an uncertainty estimator of the retrieved optical thickness τ_a by taking the standard deviation over the N_{dir} viewing directions as follows (Eq. (10)):

$$\Delta \tau_a = \sqrt{\frac{\sum_i^{N_{dir}} (\tau_{a,dir}(i) - \tau_a)^2}{N_{dir} - 1}}. \quad (10)$$

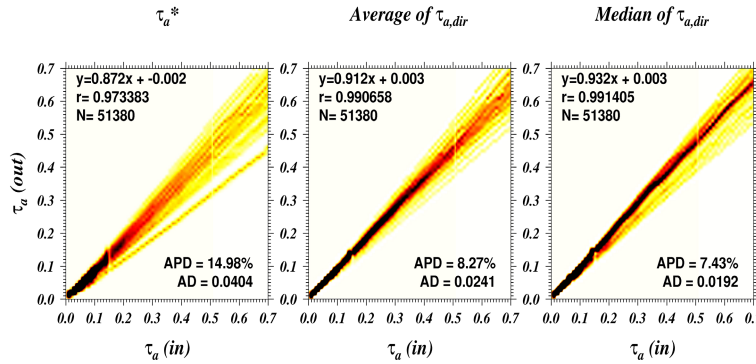


Fig. 2. Comparison between the desired aerosol optical thickness, $\tau_a(in)$, and the retrieved value $\tau_a(out)$ using three procedures: (i) τ_a^* is calculated by minimizing the multi-directional cost function J^* , (ii) average of $\tau_{a,dir}$ obtained by minimization of the mono-directional cost functions J , (iii) median value of $\tau_{a,dir}$ obtained by minimization of the mono-directional cost functions J . N : number of points, r : correlation coefficient, APD: absolute percentage difference, AD: absolute difference.

3.3.2. Aerosol model retrieval

The determination of the aerosol type by the phase (P1) of the POLAC algorithm is obtained through the minimization of the multi-directional cost function J^* computed assuming that

aerosols follow a bimodal size distribution. Based on this approach, twelve fine modes and four coarse modes of the *Laboratoire d'Optique Atmosphérique* (Université de Lille, France) aerosol models as previously defined in this paper (Table 1) are used. For each of the fine and coarse modes, a lookup table of the Stokes parameters I , Q and U at the top of atmosphere (so-called LUT-atmosphere) was generated for all the viewing configurations of the PARASOL sensor and for different aerosol optical thicknesses, τ_a . Then, the Stokes parameters Q and U at 490, 670, 865 nm and I at 865nm corresponding to any mixture of one fine and one coarse mode of aerosols are derived from the LUT-atmosphere for a given viewing configuration Ψ as follows:

$$S(\lambda, \Psi) = \gamma S^f(\tau_a(\lambda), \Psi) + (1 - \gamma) S^c(\tau_a(\lambda), \Psi) \quad (11)$$

where S^f and S^c stand for the Stokes parameter S calculated for the fine mode and the coarse mode, respectively; they are calculated for any aerosol optical thickness by linear interpolation within the LUT-atmosphere. The term γ is the mixing coefficient between the two aerosol modes (i.e., fine and coarse mode). It should be noted that Wang and Gordon [70] were the first to show that the TOA radiance contributions from fine and coarse modes can be added to determine the total TOA radiance provided that there is no absorption. This scheme was later adopted by Tanré et al. [71] to perform sensitivity studies for the retrieval of aerosol properties from the MODIS sensor. It is worth mentioning that Eq. (11) fails to accurately represent the Stokes vector of aerosol mixture when strongly absorbing aerosols are present. However, such an equation is frequently used in ocean color and aerosol remote sensing from space [26, 72] because it permits to introduce a continuous variable, namely the mixing coefficient γ , in the inversion scheme and subsequently, it enhances the number and the representativeness of the aerosol models used in that scheme. The optical thicknesses of the fine mode, τ_a^f , and of the coarse mode, τ_a^c , are then determined as follows:

$$\begin{aligned} \tau_a^f(\lambda) &= \gamma \tau_a(\lambda), \\ \tau_a^c(\lambda) &= (1 - \gamma) \tau_a(\lambda) \end{aligned} \quad (12)$$

On the basis of the Stokes parameters S determined using Eq. (11), the multi-directional cost function J^* is calculated for each couple of fine and coarse modes and different value of γ . Then, a polynomial function is used to fit the numerical values of J^* for each aerosol couple as follows:

$$J^*(\gamma) = A + B\gamma + C\gamma^2 \quad (13)$$

The minimization of $J^*(\gamma)$ provides the optimal value of the mixture coefficient, γ_{ij} , for every couple of fine mode i and coarse mode j . The couple which has the minimal value of $J^*(\gamma_{ij})$ is finally selected. At the end of this step, the aerosol model is retrieved, namely one fine mode, one coarse mode and their respective mixture represented by the γ coefficient.

3.3.3. Marine reflectance estimation

In phase (P2) of the POLAC algorithm, the LUT-ocean are used to simulate the TOA radiances and the corresponding water-leaving radiances for the atmospheric parameters retrieved by the phase (P1) and for different hydrosol types and concentrations of the water mass. As mentioned in section 3.2.2, the hydrosols are modeled for open ocean water conditions using the following couple of parameters: the chlorophyll concentration, Chl , and the exponent of the Junge size distribution, v_{phy} . For each couple of Chl and v_{phy} , the top of atmosphere Stokes parameter corresponding to the normalized radiance, I_{TOA} , is calculated using Eq. (11) for each of the viewing directions. The corresponding marine reflectance is computed simultaneously for a nadir viewing configuration over the same set of Chl and v_{phy} . The marine reflectance is calculated just beneath the sea surface as follows:

$$\rho_w(0^-) = \pi L_{u0}(0^-) / E_d(0^-) \quad (14)$$

where L_{u0} is the upwelling radiance at nadir direction and E_d is the downwelling irradiance; the notation 0^- is used to refer to the level just beneath the sea surface. Simulations of I_{TOA} and ρ_w were carried out for the visible bands of PARASOL, i.e. 490, 565 and 670 nm, except for 443 nm which is contaminated by stray-light phenomenon in PARASOL device. The use of the channel 443 nm of PARASOL sensor is not recommended by CNES [28]. The measured and simulated I_{TOA} values are used to calculate the mono- and the multi-directional cost functions J and J^* . Then a polynomial function is used to fit the numerical values of J^* as a function of ρ_w such as:

$$J^* = A + B\rho_w(0^-) + C(\rho_w(0^-))^2. \quad (15)$$

The coefficients A , B and C of Eq. (15) are obtained using the weighted least squares regression for which the weights are taken as the inverse of the variance over the entire set of viewing directions of the mono-directional cost functions J calculated for a given couple (Chl , v_{phy}). In this manner, least importance will be given to the combination of Chl and v_{phy} which induces the strongest directional dispersions. Finally, the marine reflectance is estimated by solving the polynomial of Eq. (15). An example of the marine reflectance computation step is shown Fig. 3 for an actual PARASOL pixel over the Mediterranean Sea.

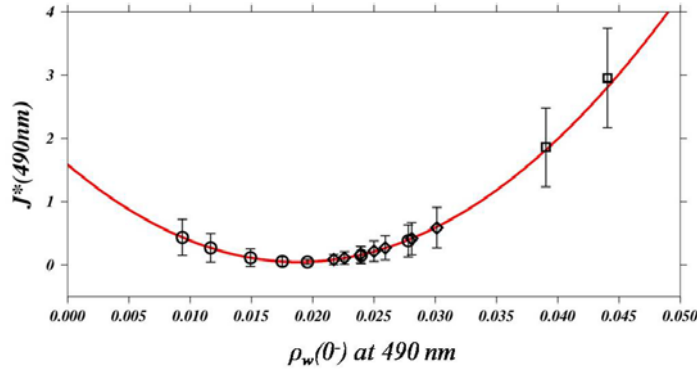


Fig. 3. Example of the marine reflectance computation step for a pixel of a PARASOL image measured at 490 nm over the Mediterranean Sea. The multi-directional cost function J^* is calculated for different chlorophyll concentrations and different Junge exponents (4.0 (diamonds), 4.5 (squares), 5.0 (circles) of phytoplankton size distribution). Then, a polynomial is used to fit the function J^* with respect to the marine reflectance $\rho_w(0^-)$. The vertical bars correspond to the standard deviation of the mono-directional cost function J over the viewing directions.

The entire inversion scheme of the PARASOL data detailed in section 3.3 leads to the retrieval of bimodal aerosol parameters and the marine reflectance at the same time. Each step of the algorithm specifically takes into account the directional information of the PARASOL data. Figure 4 summarizes the main characteristics of these steps.

3.4. Importance of Stokes parameters I , Q and U

The sensitivity of the aerosol determination to the Stokes parameters (i.e., various combinations of I , Q or U) used as inputs of the algorithm is analyzed here based on the use of the phase (P1) of the POLAC algorithm. The phase (P1) is applied to synthetic data which have been generated by the OSOA model for different couples of fine and coarse modes of aerosols. The synthetic data are combined to match the set of viewing configurations of

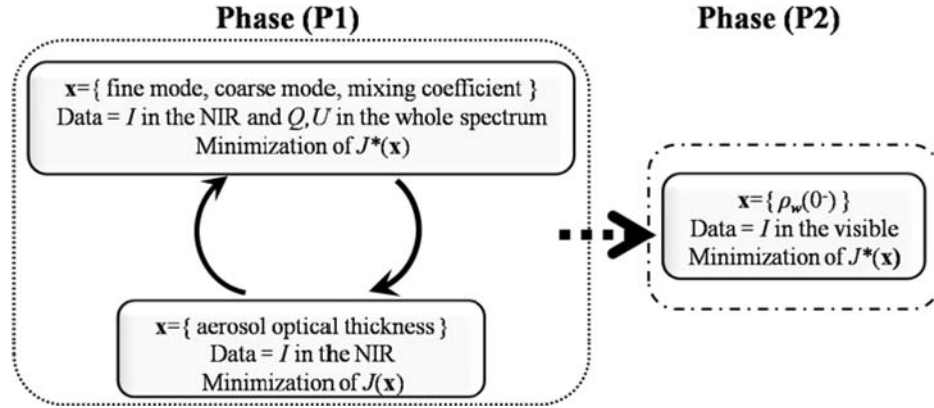


Fig. 4. Schematic diagram of the different steps of the POLAC algorithm. For each step, the vector \mathbf{x} of the parameters which need to be retrieved, the PARASOL data and the directional cost function used are mentioned in the figure. NIR means the near-infrared part of the spectrum, ρ_w is the nadir marine reflectance just beneath the sea surface, the functions J and J^* are the mono- and multi-directional cost functions, respectively.

PARASOL pixels. The spectral variation of a given aerosol model is often quantified using the Angstrom exponent α_{ang} [73, 74], as defined by

$$\alpha_{ang}(\lambda, \lambda_{ref}) = \ln \left(\frac{\tau_a(\lambda_{ref})}{\tau_a(\lambda)} \right) * \left[\ln \left(\frac{\lambda}{\lambda_{ref}} \right) \right]^{-1}, \quad (16)$$

Although Eq. (16) is a rough parameterization, the value of the Angstrom exponent is often used to characterize the maritime, biomass burning or urban aerosol components [75, 76], mainly because it could be easily measured. Typically, low values of α_{ang} indicate the predominance of coarse aerosols relative to the fine mode, and *vice versa*. Furthermore, the accuracy of the atmospheric correction relies on the good retrieval of the aerosol spectral behavior and thus, it relies on the correct estimation of α_{ang} . The Angstrom exponent of the aerosol models is used hereafter to evaluate the performance of the aerosol determination from the Stokes parameters. Simulations of synthetic data were carried out for a large number of fine and coarse mode aerosol mixtures which provides a wide range of Angstrom exponents ranging from -0.02 (extra-large particles) up to $+3.0$ (ultra-fine particles).

The POLAC algorithm was applied to the entire synthetic data set simulated for a given Angstrom exponent noted $\alpha_{ang}(in)$. The exponent estimated by the algorithm is then noted $\alpha_{ang}(out)$. Three different combinations of Stokes parameters were used in POLAC algorithm to determine the aerosol models: (i) I at 865 and 1020 nm, (ii) Q and U at 490, 670 and 865 nm, (iii) the combination of (i) and (ii). For those three combinations, the retrieved values of $\alpha_{ang}(out)$ are shown with respect to the desired exponent $\alpha_{ang}(in)$ for a solar viewing zenith angle of 30° and an aerosol optical thickness value of 0.1 (Fig. 5) and 0.5 (Fig. 6) at 550 nm. For each combination and both turbidities, $\alpha_{ang}(out)$ and $\alpha_{ang}(in)$ are highly correlated with a correlation coefficient greater than 0.95. However, the highest dispersion occurs for the combination (i), which makes use of the parameter I only, where an absolute percentage difference (APD) value of 55% and 40% is obtained in clear and turbid atmosphere conditions, respectively. The aerosol determination based on the sole radiometric measurements of I at two distinct near-infrared wavelengths fails depending on the aerosol properties to be retrieved. In fact, similar radiance values at those two wavelengths might be generated by the interaction of light with different aerosol types whereas the corresponding radiances at the shorter wavelengths are different. Previous studies already highlighted this feature and concluded to the necessity of accounting for the second order of the Angstrom

law, called curvature, to improve the modeling of the spectral behavior of the aerosols [77, 78]. The particularly pronounced curvature of fine modes can explain the discrepancies of the retrievals when the combination (i) is used. Conversely, the best agreement between $\alpha_{ang}(out)$ and $\alpha_{ang}(in)$ are obtained for the combination (ii) (APD is lower than 7.1%) for which only the polarized Stokes parameters Q and U are used. The simultaneous use of the three Stokes parameters, i.e. combination (iii), is an intermediate case showing that the polarized information of Q and U is not used as efficiently as the case (ii) by the algorithm. The introduction of I in the case (iii) is not correctly handled by the algorithm because more relevant information on the optical signature of aerosols is contained in the polarized radiance (i.e., Q and U) than in the scalar radiance.

The analysis of the influence of the turbidity on the performance of the algorithm (comparison of Fig. 5 and Fig. 6) shows that for each combination, the APD is significantly reduced when the atmosphere is more turbid. Such an improvement of the performance of POLAC was expected since aerosols increasingly contribute to the atmospheric radiance in turbid cases. For example, the APD decreases by one order of magnitude (from 42% for $\tau_a = 0.1$ (Fig. 5) to 4.5% for $\tau_a = 0.5$ (Fig. 6)) in the case (iii) when the atmosphere becomes more turbid. As a comparison, the decrease of APD with turbidity is less pronounced for the combination (i) (from 55% (Fig. 5) to 40% (Fig. 6)). The combination (ii) remains the most

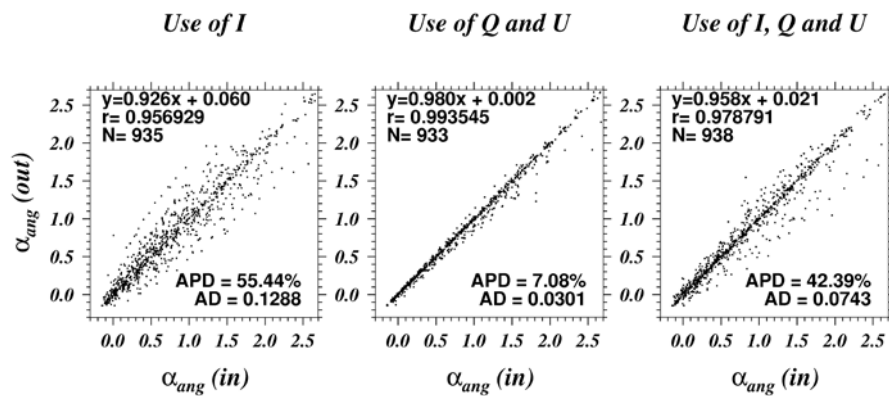


Fig. 5. Comparison between the desired Angstrom exponents, $\alpha_{ang}(in)$, and the exponents retrieved by the algorithm, $\alpha_{ang}(out)$, when three different combinations of the Stokes parameters are used as inputs to the algorithm for clear atmosphere conditions (aerosol optical thickness of 0.1 at 550nm). The following spectral bands have been used for the retrievals: 865 nm for I and 490, 670 and 865 nm for Q and U.

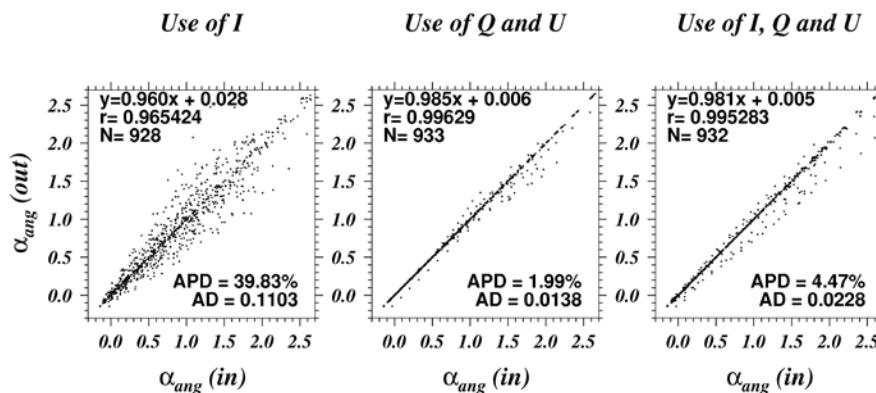


Fig. 6. Same as Fig. 5 for moderately turbid atmosphere conditions (aerosol optical thickness of 0.5 at 550 nm).

accurate combination (APD < 2%) to determine the aerosol model in turbid conditions. The aerosol contribution to the atmospheric signal, especially their contribution to the polarized signal (i.e., Q and U) is quantitatively higher than for clear atmospheres (that is mainly explained by the higher proportion of multiple scattering in turbid conditions). Therefore, the information contained in Q and U is more efficiently used by POLAC in turbid cases. The information contained in I is widely used to estimate the aerosol optical thickness rather than the aerosol model characteristics (e.g., Angstrom exponent). In summary, the information contained in the total radiance I is mainly exploited to retrieve the aerosol optical thickness while the aerosol model properties such as the spectral characteristics of aerosols is mostly determined based on the polarized information.

3.5. Importance of the polarized information at short wavelengths of the visible spectrum

In this section, the influence of the polarized information at short wavelengths, namely at 490 nm, on the performance of the retrieval of aerosol type by POLAC is analyzed. Note that, for that purpose, only the Stokes parameters Q and U are used in the aerosol model determination step. The POLAC procedure is applied for the three following combinations of PARASOL bands: (i) 490 nm only, (ii) 670 and 865 nm, (iii) all the available PARASOL polarized bands: 490, 670 and 865 nm. The results are displayed for clear atmosphere (Fig. 7) and moderately turbid atmosphere (Fig. 8) conditions. In every case, the retrieved Angstrom exponents, $\alpha_{ang}(out)$, are strongly correlated to the desired exponents, $\alpha_{ang}(in)$. The correlation coefficient is greater than 0.99. Such high values of the correlation coefficient highlight the ability of determining accurately the aerosol spectral behavior using only one spectral band, at 490 nm for instance.

For the clear atmosphere case (Fig. 7), the absolute percentage difference (APD) between $\alpha_{ang}(out)$ and $\alpha_{ang}(in)$ when the sole band 490 nm is used (APD = 3.3%) is lower than that which uses the bands at 670 and 865 nm (APD = 4.8%). Similar results are obtained for the moderately turbid atmosphere condition (Fig. 8) (APD decreases from 1.8% to 1.4% from the case of the bands 670, 865 nm to the case of the sole band 490 nm). For most of the real-world conditions, the Angstrom exponent is positive, and the magnitude of the aerosol signal is higher at short wavelengths. Furthermore, the oceanic polarized signal is independent of phytoplankton concentration at short wavelengths [17]. Therefore, Q and U parameters at 490 nm are highly informative on aerosol optical properties. Subsequently, the use of Q and U parameters at 490 nm increases the performance of determination of aerosol type rather than the use of Q and U at longer wavelengths. It should be highlighted that the use of the 490nm-

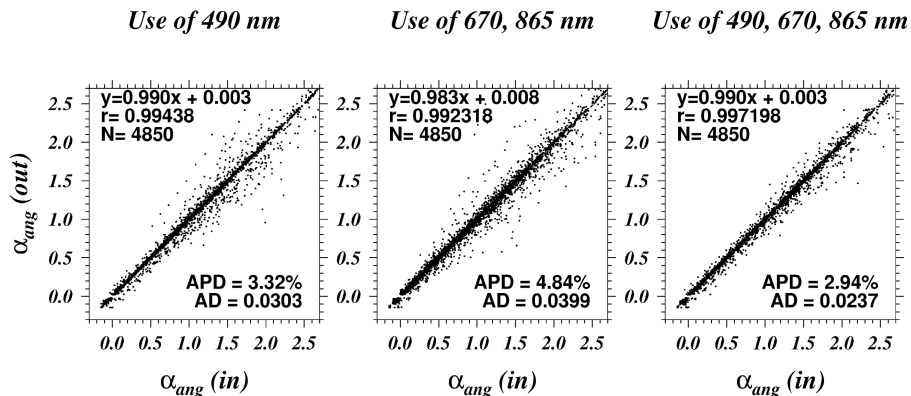


Fig. 7. Comparison between the desired Angstrom exponents, $\alpha_{ang}(in)$, and the exponents retrieved by the algorithm, $\alpha_{ang}(out)$, when the Stokes parameters Q and U are used as inputs to the algorithms for three different combinations of PARASOL bands. Clear atmosphere conditions (aerosol optical thickness of 0.1 at 550nm).

Use of 490 nm

Use of 670, 865 nm

Use of 490, 670, 865 nm

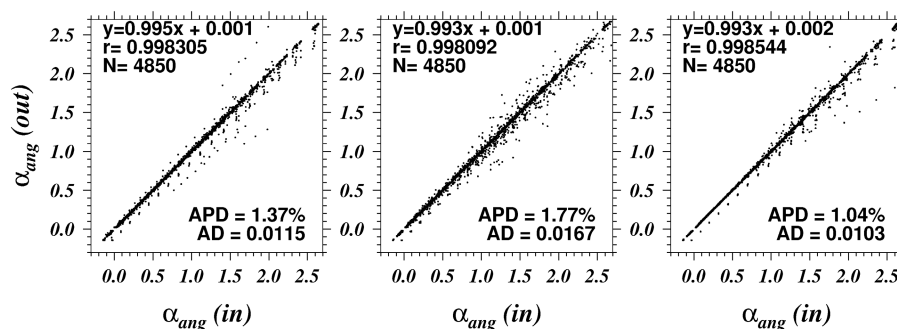


Fig. 8. Similar to Fig. 7 but for moderately turbid atmosphere conditions (aerosol optical thickness of 0.5 at 550nm).

band determines more accurately the presence of fine mode aerosols, which are characterized by high values of α_{ang} , than the use of red/near infrared wavelengths. This point is consistent with other studies; see [79] for instance. The comparison between the clear and turbid cases (Fig. 7 and Fig. 8) shows that APD is roughly divided by a factor of 3 for each spectral combination. Again, such a decrease of APD with turbidity is explained by the fact that the aerosol signal is significantly amplified for turbid atmospheres and thus, the aerosol optical signature is more pronounced.

These results show that a sensor that would have only one polarized band in the blue part of the spectrum can still be exploited to efficiently determine the aerosol type. The implications for designing a forthcoming satellite sensor and for reducing the cost of a satellite mission are important since one polarized band at short wavelength should be sufficient to derive accurate aerosol optical properties for clear and turbid atmospheres.

The use of the three PARASOL polarized bands together induces a significant decrease of AD and APD for both clear (Fig. 7) and turbid atmosphere conditions (Fig. 8). Thus, the information of each polarized spectral band can be merged to improve the aerosol type determination. The use of Q and U at 490 nm in addition to the use of Q and U at 670 nm and 865 nm leads to improve by more than 35% (i.e. $[AD(ii)-AD(iii)]/AD(ii)$) the accuracy of Angstrom exponent retrieval and therefore the aerosol type determination. The most important results of this theoretical study can be summarized as follows. First, the polarized information at 490 nm is sufficiently accurate to estimate the Angstrom exponent with an uncertainty lower than 4%. Second, Q and U at 490nm can be used to improve the determination of the fine aerosols over open ocean regardless of the hydrosol concentration [18]. Finally, the spectral information of the polarized Stokes parameters can be merged to improve the aerosol detection. It should be noted that the optimal performance of the POLAC algorithm applied to the PARASOL data was assessed here theoretically. So, it is likely that the geophysical noise existing in the measurements will reduce the performances of the algorithm. However, this theoretical analysis based on PARASOL characteristics concludes that it is highly recommended to introduce a polarimetric channel in the blue part of the spectrum onboard future satellites platform since it will significantly improve the aerosol type detection and consequently, the aerosol optical thickness retrieval.

4. Influence of the polarized information on water-leaving radiance retrieval

4.1. Theoretical performance of the water-leaving radiance retrieval

Synthetic data were simulated using the radiative transfer model OSOA for numerous geometrical configurations. The calculation of Stokes parameters I , Q and U for each viewing

direction and each spectral band of PARASOL sensor enables to generate a synthetic PARASOL-like image. Each pixel of this image correspond to a given aerosol optical thickness, aerosol model and concentration of phytoplankton of the oceanic layer. The POLAC algorithm is applied to those synthetic pixels in order to retrieve the nadir marine reflectance just beneath the sea surface as defined in Eq. (14). The PARASOL Level 1 data are originally corrected from the instrumental noise as well as from stray light [80]. However, other types of noise might affect the satellite data such as those which originates from the radiometric calibration or from the overall remotely sensed scene itself [28]. This geophysical noise was here simulated using two white Gaussian noises. One of these Gaussian noises represents a directional noise, referred to as B_ψ , which is only dependent on the viewing configuration. The other one represents a spectral noise, referred to as B_λ , which is only dependent on the spectral band used. Those realistic noises were then applied to the simulated Stokes parameters as follows:

$$S_i^{synth}(\Psi, \lambda) = (1 + B_\psi B_\lambda) S_i^{sim}(\Psi, \lambda) \quad (17)$$

where S^{sim} is the “noise-free” Stokes parameter (i.e., I , Q or U) simulated using the radiative transfer computations and S^{synth} is the “noisy” Stokes parameter used to generate the synthetic PARASOL-like pixels. Spectral noise produces a bias which is spectrally variable. Note that this bias is similar for all the viewing direction. Based on this definition, the spectral noise is comparable to the effects produced by non-ideal radiometric calibration and, to a lesser extent, by the presence of foam on the sea surface [81, 82]. On the other hand, the directional noise allows taking into account the noise which contaminates each directional acquisition separately such as the effect of contamination by the sun glint or thin clouds in the measurements. It is assumed that B_ψ and B_λ are not independent from each other. Therefore, the noise was modelled as a multiplication of these two components, as written in Eq. (17).

The estimation of the marine reflectance is carried out by the phase (P2) of the POLAC algorithm based on the atmospheric parameters retrieved through phase (P1). To evaluate the performances of the entire algorithm, the synthetic data S^{synth} were simulated for different aerosol models for an optical thickness value of 0.1 at 550nm and the following oceanic parameters: chlorophyll concentration ranging from 0.03 to 10.0 mg m⁻³, Junge exponent of phytoplankton size distribution ranging from 3.5 to 4.5. Those synthetic data were simulated for various solar zenith angles from 30° to 60°. In addition, the nadir marine reflectances $\rho_w^-(in)$ were calculated at 490, 565 and 670 nm for each set of those input parameters. The POLAC algorithm is eventually applied to the PARASOL-like synthetic data to estimate the nadir marine reflectances $\rho_w^-(out)$. The comparison between the desired reflectance $\rho_w^-(in)$ and the retrieved reflectance $\rho_w^-(out)$ is then carried out with or without geophysical noise (Fig. 9). A noise value of 1% is applied to all the Stokes parameters at the top of atmosphere used in both phases (P1) and (P2) of the algorithm. It should be noted that realistic values of the geophysical noise should not be much greater than 1% as pointed out by previous studies dealing with vicarious calibration of ocean color radiometry satellites [28, 83].

In every presented case, $\rho_w^-(out)$ is highly correlated with the expected marine reflectance $\rho_w^-(in)$ following the 1:1 line with a correlation coefficient greater than 0.95 for the three spectral bands considered (Fig. 9). The residual dispersion of the algorithm, which corresponds to the value of the APD for the “noise-free” case, is around 1% (top of Fig. 9, case noise = 0%). The estimation of the marine reflectance by the algorithm is unbiased (i.e. offset of the regression line ~0). The addition of a realistic noise of 1% induces a slight degradation of the retrieval performances, APD < 3%, for the bands at 490 and 565 nm (bottom of Fig. 9, case noise = 1%). It should be noted that larger dispersion in the retrieval occurs at 565 nm around reflectances of 0.022. This can be explained by the very low sensitivity of the signal at 565 nm to variations in the Chlorophyll-a concentration. In

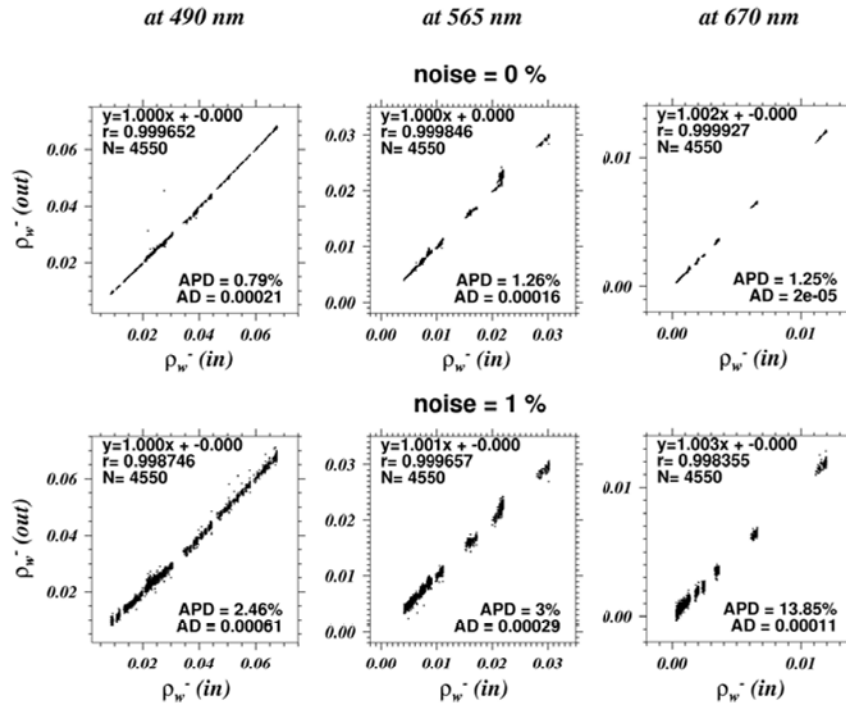


Fig. 9. Comparison between the desired nadir subsurface marine reflectances $\rho_w^-(in)$ and the retrieved ones $\rho_w^-(out)$ for synthetic pixels contaminated by spectral and directional noise values of 0% and 1% respectively. The pixels were simulated for different aerosol models with an optical thickness of 0.1 at 550 nm.

particular, Harmel [84] showed that the impact of a Chlorophyll-a variation from 0.03 to 0.1 $mg\ m^{-3}$ on the top-of-atmosphere signal is smaller than the radiometric accuracy of the PARASOL sensor. On the other hand, the value of the marine reflectance at 565 nm for this range of Chlorophyll-a concentration is around 0.022 where the larger dispersion can be seen. Thus, the “bumps” as observed in Fig. 9 at 565 nm are most likely related to the satellite sensor performance rather than artefacts of the LUT method. The dispersion of ρ_w^- at 670 nm is greater than 5%, which is the value required for the ocean color radiometry applications [85]. However, note that the magnitude of the marine reflectance at 670 nm is very low and the absolute difference AD at this wavelength is significantly lower than that observed at the shorter wavelengths. The satisfactory results obtained when the value of the noise is 1% confirm the ability and the high potential of POLAC to accurately estimate the water-leaving radiance from the multidirectional and polarized data of PARASOL over oceanic waters with a theoretical uncertainty lower than 3% for the 490 and 565 nm bands.

4.2. Application to PARASOL images

The POLAC algorithm was applied to several PARASOL level 1 images selected around the world over open ocean waters. For convenience, the following analysis was carried out based on a single PARASOL image acquired on May 5th 2006 over the Mediterranean Sea. It is worth noting that similar results were obtained when considering a large set of PARASOL images over Atlantic and Pacific Oceans. The PARASOL image acquired on May 5th 2006 was selected because it exhibits significant variability of both atmospheric and oceanic parameters throughout the entire scene. In particular, the aerosol optical thickness retrieved by SeaWiFS mission for the same day exhibits areas of very clear ($\tau_a < 0.07$ at 865nm) and slightly turbid atmosphere ($\tau_a \sim 0.18$ at 865nm), see Fig. 10.(a). The aerosol optical thickness

retrieved by POLAC from the level 1 PARASOL image shows similar patterns as SeaWiFS image over the whole scene. However, the POLAC aerosol optical thickness values are significantly higher (Fig. 10.(c)). This difference can be explained by the better ability of POLAC to detect the fine aerosols using the polarized information in the visible part of the spectrum as previously shown. Thus, the additional contribution of these fine aerosols to the optical thickness as accounted for in POLAC method leads to an increase of the total τ_a relatively to the value retrieved by SeaWiFS. The chlorophyll concentrations, *Chl*, were obtained through the algorithms OC4v4 and OC2v2 [86] applied to the SeaWiFS and PARASOL water leaving radiances, respectively. The *Chl* images derived from SeaWiFS and POLAC-PARASOL data (Fig. 10.(b) and (d), respectively) show the presence of a significant bloom patch at latitude 42°N (the chlorophyll concentration is greater than 2 mg m⁻³). Such a pattern is typical of the spring bloom occurring in that area [87]. It should be noted that an oligotrophic area located south of the bloom area is detected by both SeaWiFS and POLAC algorithms; however, the concentrations retrieved by POLAC are significantly lower than those retrieved by SeaWiFS. It is worth noting that these discrepancies are consistent with those observed in the water leaving radiance products and are therefore independent of the use of the slightly different algorithms OC4v4 and OC2v2. Same qualitative analyses were carried out over several PARASOL and SeaWiFS images around the world (not shown), and it can be concluded that the POLAC retrievals are meaningful and comparable to the other ocean color radiometry missions.

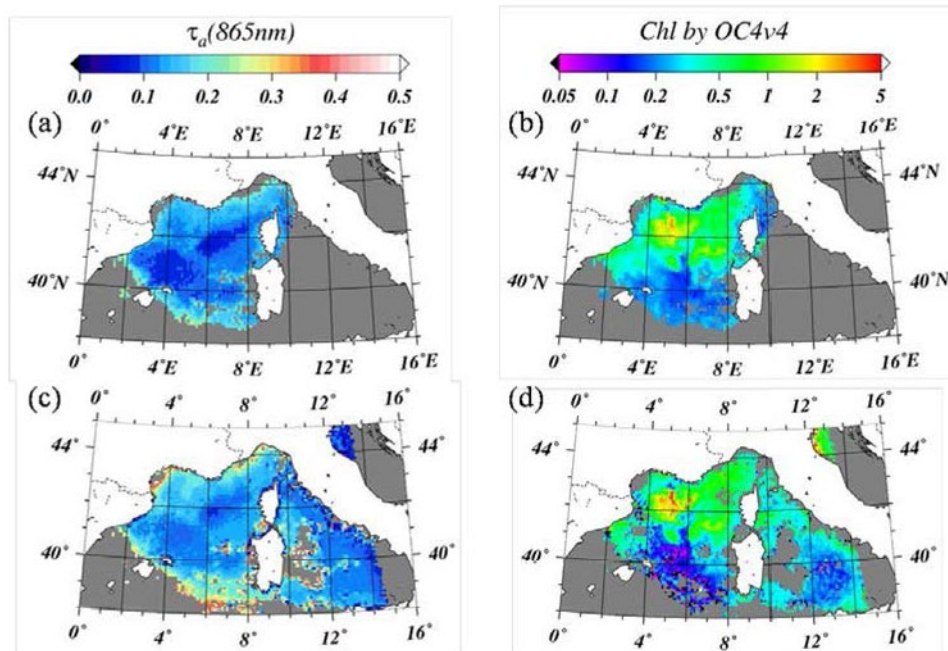


Fig. 10. Level 2 satellite images acquired on May 5th 2006 over the Mediterranean Sea. (a) SeaWiFS Aerosol optical thickness at 865nm and (b) SeaWiFS chlorophyll concentration in mg m⁻³, (c) Aerosol optical thickness at 865nm as derived by POLAC applied to the level 1 PARASOL image (d) chlorophyll concentration in mg m⁻³ as derived by POLAC applied to the level 1 PARASOL image. The chlorophyll concentration is calculated using the SeaWiFS OC4v4 (OC2v2 for PARASOL data) algorithm based on the retrieved water-leaving radiances.

The POLAC algorithm can now be used to evaluate the importance of the polarized information to estimate the water leaving radiances from top of atmosphere measurements. For this purpose, two modified versions of POLAC were applied to PARASOL images. The first one, so-called POLAC_{NOPOL}, does not make use of the polarized information at all; only

the Stokes parameters I (i.e. total radiance at 865 and 1020 nm) are used for the aerosol type determination. The second version of POLAC, so-called POLAC_{NOVIS}, makes use of Q and U at 670 and 865 nm to determine the aerosol type instead of 490, 670 and 865 nm in the original version. Those two modified versions of POLAC were applied to the selected level 1 PARASOL image. The normalized water-leaving radiances nL_w at 490 nm obtained with POLAC_{NOPOL}, POLAC_{NOVIS} and POLAC are shown on Fig. 11.(a), (b) and (c), respectively. Those results can be compared with the normalized water-leaving radiances retrieved at the same wavelength by the SeaWiFS sensor (Fig. 11.(d)). The values of nL_w at 490 nm are highly overestimated by POLAC_{NOPOL} relatively to the SeaWiFS retrievals with values greater than $1.5 \text{ mW cm}^{-2} \mu\text{m}^{-1} \text{sr}^{-1}$ (Fig. 11.(a)). In addition no distinct patterns are visible over the image. It was shown earlier in this paper that this version of POLAC, which makes use only of I to determine the aerosol type, fails to detect the fine aerosols. Therefore, the atmospheric signal is particularly underestimated at short wavelengths where the fine mode is optically predominant and subsequently the oceanic signal is amplified.

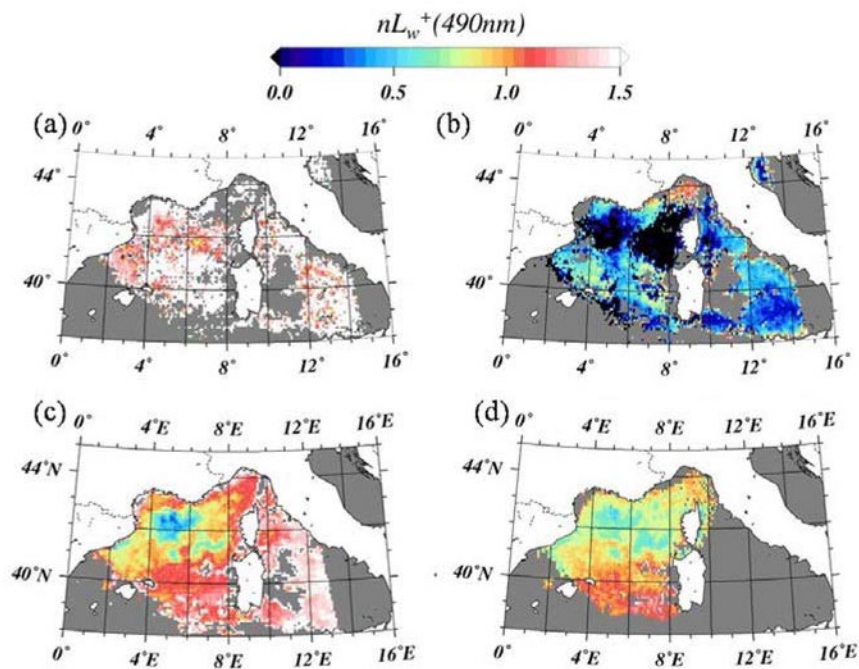


Fig. 11. Normalized water-leaving radiances nL_w at 490 nm (in $\text{mW cm}^{-2} \mu\text{m}^{-1} \text{sr}^{-1}$) retrieved by the modified versions of POLAC using the level 1 PARASOL image acquired on May 5th 2006 over Mediterranean Sea (a) POLAC_{NOPOL} (b) POLAC_{NOVIS} and (c) the original version of POLAC, (d) level 2 SeaWiFS image of nL_w at 490 nm over the same area.

The version POLAC_{NOVIS}, which makes use of the polarized information in the red/near infrared bands only, leads to underestimations of the water-leaving radiance and sometimes to negative values (Fig. 11.(b)). However, it has been verified that the chlorophyll concentrations calculated from the positive values of nL_w are consistent with the bloom patch and with the location of the southern oligotrophic area, which is centered on 40°N and 5°E . Such consistency is not observed when POLAC_{NOPOL} is applied. The use of Q and U at all wavelengths (Fig. 11.(c)) as an alternative to Q and U at 670 and 865 nm (Fig. 11.(b)) increases significantly the performances of the retrieval of the ocean color radiometry from space. The better consistency of the retrievals supplied by the original version of POLAC, which makes use of the additional information of Q and U at 490 nm, emphasizes the high

potential and benefits of using this channel for the atmospheric correction over open ocean. It should be reminded that our results showed that the additional use of Q and U at 490 nm theoretically improves the aerosol type determination by 35%. The results obtained here based on actual measurements confirm the spectral complementarities of the polarized information to advantageously determine the aerosol characteristics. The inaccurate aerosol determination supplied by POLAC_{NOPOL} and POLAC_{NOVIS} is therefore the first factor to explain the unsatisfactory retrieval of water leaving radiances. That point highlights the high sensitivity of our atmospheric correction algorithm, which retrieves simultaneously atmospheric and oceanic parameters, to the aerosol characteristics retrievals. Such a high sensitivity is one of the main limitations of the POLAC algorithm. However, this difficulty can be overcome either by the enhancement of the radiometric accuracy or by adding more polarized band to future sensors. Those preliminary results demonstrate the efficiency of the use of directional and polarized measurements to carry out atmospheric correction over open ocean. The satisfactory performances of the POLAC algorithm allow contemplating accurate retrieval of the water leaving radiance and the fine and coarse aerosol modes simultaneously.

5. Conclusions and perspectives

A specific atmospheric correction algorithm, so-called *multi-directionality and POLarization-based Atmospheric Correction* (POLAC), was proposed. This algorithm relies on the exploitation of the multidirectional and polarized properties of the top of atmosphere signal as measured by the satellite sensor PARASOL. POLAC algorithm is composed of two principal phases. Aerosol optical properties retrieval is carried out in the first phase and the derivation of the water leaving radiance is performed in the second phase. POLAC thus enables to simultaneously retrieve atmospheric and oceanic optical parameters. Those two phases make use of an optimization scheme between the PARASOL-like measurements and forward simulations of the radiative transfer in the coupled atmosphere-ocean system to retrieve the geophysical parameters of interest. The first phase (P1) is dedicated to the inversion of the PARASOL radiance and polarization data which are insensitive to the in-water constituents for retrieving the aerosol optical properties. These aerosol optical properties are determined based on the information contained in the radiance (i.e. Stokes parameter I) in the near-infrared (NIR) only and the information contained in the Stokes parameters Q and U in the visible and NIR region. The phase (P1) is subdivided into two iterative steps; one step makes use of Q and U for retrieving the best bimodal aerosol model defined by a couple of a fine mode and a coarse mode as well as their respective proportion, while the other step is dedicated to the estimation of aerosol optical thickness. In such iterative procedure, the convergence of the retrieved values is obtained typically after 2 or 3 iterations. Based on the outputs of (P1), the phase (P2) carries out the water-leaving radiance retrieval in the visible spectrum (e.g. 490, 565, 670 nm) by matching the TOA radiance measurements with radiative transfer simulations computed for various hydrosol compositions of the oceanic layer. The influence of directional information of PARASOL-like data on the performance of POLAC was analyzed. It has been shown that the aerosol optical thickness is better estimated when a mono-directional approach is used whereas a multi-directional approach is more efficient to determine the fine and coarse modes of the aerosol model.

The sensitivity of the retrieval of aerosol optical properties to different combinations of Stokes parameters used in POLAC was studied. Our results show that POLAC theoretical accuracy for deriving the Angstrom exponent is around 3% and 1% in clear and turbid atmospheric conditions, respectively. Subsequently, our study pointed out that the use of the polarized Stokes parameters Q and U significantly improves the aerosol type determination while the simultaneous use of the total radiance I together with Q and U parameters does not improve the aerosol type determination. In addition, the use of the sole polarized information at 490 nm is efficient to estimate the Angstrom exponent with an uncertainty lower than 4%. The introduction of Q and U at 490 nm in POLAC algorithm induces a reduction by 35% of

the accuracy of Angstrom exponent estimation. The use of Q and U at 490 nm also specifically improves the determination of the fine mode of aerosols over open ocean regardless of the phytoplankton concentration.

The algorithm was then applied to numerous level 1 PARASOL images. The influence of the polarized information on the retrieval of geophysical products was studied based on these images. It was shown that the use of the polarimetric data increases significantly the performance of detection of the aerosols, thus confirming the theoretical sensitivity study. Consequently, the atmospheric signal is reappraised improving *de facto* the water leaving radiance estimation. Our analysis highlighted the high sensitivity of the estimated water leaving radiances to the aerosol model determination by the algorithm. The exact quantification of that sensitivity is one of the perspectives of this study. However, the satisfactory performances of the POLAC algorithm demonstrated the feasibility to perform determination of a couple of fine and coarse modes of aerosols and derivation of the water leaving radiance based on a relevant exploitation of multidirectional and polarimetric PARASOL data.

This study has shown the ability of the original POLAC algorithm to achieve atmospheric correction and aerosol retrieval over open ocean. A direct perspective of this work is to make use of the POLAC algorithm to investigate the requirements of the future NASA mission so-called Aerosols, Clouds and Ecosystems (ACE) and its preparatory mission (PACE), scheduled for launch around 2018. Since those two missions will include a multidirectional polarimeter instrument, results provided in this paper should greatly contribute to make optimal the future exploitation of the ACE/PACE data. Note that if ACE/PACE polarimeter is not multi-angle and contains only one polarization measurement per field of view, the accuracy of the retrieval of aerosol optical thickness and of the aerosol model determination might be significantly degraded in comparison to multidirectional systems. This is because the polarized information is highly sensitive to the viewing geometry (i.e. viewing and solar angles as well as relative azimuth). As a result, the amount of useful information contained in mono-directional polarization measurements would be significantly dependent on the latitude of observation and on the period of the year. Thus, it can be recommended to include multi-directional polarized sensors to properly exploit the polarization property of light. If this latter condition could not be satisfied for some reasons, we think that, at least, a mono-directional sensor should be designed to adjust the viewing observation angle of the polarization sensor with respect to the Sun position along the satellite orbit to make sure that the magnitude of the polarization signal will be sufficiently high to derive aerosol optical properties (e.g. ideally, the range of scattering angle for observations should be within 90° - 135°).

Further works are also required to validate POLAC performances using *in situ* data. A current work is in progress to compare the POLAC retrieval of aerosol properties with a large set of AERONET aerosol product [88]. Similar work is being conducted for the validation of water leaving radiances using temporal series of the BOUSSOLE buoy moored in the Mediterranean Sea [16] and MOBY buoy off Lanai, Hawaii [89]. Then, the processing of the entire PARASOL data set collected since it was launched (more than seven years ago) will offer a basis to take into account the overall benefits of the polarized information to monitor the aerosol, the water leaving radiance and thus, phytoplankton biomass variations at global scale.

Acknowledgments

This research was supported by Centre National d'Etudes Spatiales (CNES) and by ACRI-ST Company through the doctoral fellowship of Tristan Harmel. The authors would like to thank the organization ICARE (Laboratoire Optique Atmosphérique and CNES) for providing the PARASOL geophysical products. The authors also wish to thank Alex Gilerson and Alberto Tonizzo of the City College of New York for their helpful comments and suggestions. We would like to thank the reviewers for their relevant comments and suggestions.